NIH Public Access
Author Manuscript
Opt Express. Author manuscript; available in PMC 2009 November 30.

Published in final edited form as:
Opt Express. 2009 September 14; 17(19): 16957–16968.

Performance of reduced bit-depth acquisition for optical frequency domain imaging

Brian D. Goldberg[1,2], **Benjamin J. Vakoc**[1,2], **Wang-Yuhl Oh**[1], **Melissa J. Suter**[1], **Sergio Waxman**[3], **Mark I. Freilich**[3], **Brett E. Bouma**[1,2], and **Guillermo J. Tearney**[1,2,*]

[1]Wellman Center for Photomedicine, Massachusetts General Hospital, 50 Blossom St., Boston, MA 02114

[2]Harvard-MIT Division of Health Sciences and Technology, 77 Massachusetts Avenue, Cambridge, MA 02139

[3]Department of Cardiology, Lahey Clinic, 41 Mall Road, Burlington, MA 0180

Abstract

High-speed optical frequency domain imaging (OFDI) has enabled practical wide-field microscopic imaging in the biological laboratory and clinical medicine. The imaging speed of OFDI, and therefore the field of view, of current systems is limited by the rate at which data can be digitized and archived rather than the system sensitivity or laser performance. One solution to this bottleneck is to natively digitize OFDI signals at reduced bit depths, e.g., at 8-bit depth rather than the conventional 12–14 bit depth, thereby reducing overall bandwidth. However, the implications of reduced bit-depth acquisition on image quality have not been studied. In this paper, we use simulations and empirical studies to evaluate the effects of reduced depth acquisition on OFDI image quality. We show that image acquisition at 8-bit depth allows high system sensitivity with only a minimal drop in the signal-to-noise ratio compared to higher bit-depth systems. Images of a human coronary artery acquired *in vivo* at 8-bit depth are presented and compared with images at higher bit-depth acquisition.

1. Introduction

Optical frequency domain imaging (OFDI) [1], also known as swept-source OCT [2], is a high-resolution (~10 μm), cross-sectional, fiber-optic imaging method that is capable of measuring tissue microstructure, birefringence [3,4], and blood flow [5,6]. The most important feature of OFDI, however, is its very fast image acquisition speed, which enables wide-field imaging studies *in vivo* [7–9]. Since the interferometric ranging signal in OFDI is collected in the Fourier domain, high-speeds can be achieved while maintaining sufficient detection sensitivity [2,10, 11]. With the advent of rapid-scanning wavelength-swept lasers [12–15], the speed of clinically-viable OFDI systems is currently limited by digital acquisition and storage capabilities. The relationship between imaging speed and the required digital throughput is determined by several factors, but the minimum necessary sampling rate is generally given by $f_A * N$ where f_A is the A-line rate and N is the number of points per A-line. N is given by $2*\Delta\lambda/\delta\lambda$ and $\Delta\lambda$ *and* $\delta\lambda$ are the wavelength sweep range and instantaneous line-width of the laser, respectively. In addition, polarization diversity or polarization-sensitivity is highly desirable for robust clinical systems and doubles the required digital throughput.

©2009 Optical Society of America

*gtearney@partners.org.

OCIS codes: (170.4500) Optical Coherence Tomography; (170.3890) Medical optics instrumentation; (110.4280) Noise in imaging systems

NIH-PA Author Manuscript
NIH-PA Author Manuscript
NIH-PA Author Manuscript

NIH-PA Author Manuscript

NIH-PA Author Manuscript

NIH-PA Author Manuscript

In order to preserve the inherent dynamic range of OFDI, systems have typically utilized 12, 14 or 16 bit-depth digitizers. A typical polarization-diverse system, based on an 100 kHz repetition rate laser, capable of generating 195 images per second (512 A-lines per image), would therefore require a data throughput rate of 819.2 MB/s at 2048 points per A-line and assuming each sample is transferred as a two byte (16 bit) word. Clinical imaging with such a system may generate total data volumes in excess of 100 GB per patient and ten's of terabytes per study. Lowering the bit depth of acquisition would be a simple strategy for reducing data rates and volumes while also making it possible to utilize a broader range of fast digital acquisition electronics.

We have therefore investigated whether 8-bit sampling can be used without inhibiting image quality. In order to reduce the data transfer demand, lower bit-depth data acquisition boards (DAQ) could be used. However, the tradeoffs between sensitivity, dynamic range, and bit-depth have not been thoroughly investigated, making it difficult to justify and or evaluate reduced bit-depth systems. Prior analyses of the sensitivity of Fourier Domain OCT systems typically assume the system is designed such that DAQ noise terms can be ignored [2,11], or have explicitly stated that the quantization noise is minimized by the choice of detector gain [12]. Previously it has been suggested that high bit-depth DAQ boards are required for imaging through scattering tissue with high dynamic range [16]. Some groups have used 8-bit digitization for faster acquisition and lower cost and achieved a 52 dB dynamic range [17]. *Huber et. al.* also used an 8-bit osilliscope at 5GS/s in order to compare 8 and 14 bit-depth images [18]. They achieved an image contrast of 37 dB in the 8 bit image, but a formal noise analysis was not presented. Here, we present a formal noise analysis of an OFDI system including the effects of bit-depth on signal quantization noise. We digitize OFDI signals at various bit-depths to analyze the effect on sensitivity and dynamic range, and compare these results with a theoretical model of OFDI that includes quantization noise. Our results show that a true 8-bit data acquisition system can achieve high system sensitivity and dynamic range with only a minimal drop in the signal-to-noise ratio. *In*-vivo images of a human coronary demonstrate no significant differences between images acquired at 8- and 14-bits suggesting that 8-bit DAQ boards can be used to increase imaging speeds in clinical OFDI systems.

2. Principles

In order to understand the impact of reduced bit-depth acquisition on OFDI image quality, the following set of experiments were conducted. First, a full treatment of the non-quantization dependent noise terms in OFDI including optical, electrical, and DAQ noise was developed, modified from prior works [2,10–12,19] to include quantization noise. These noise terms were then experimentally confirmed using an high bit-depth OFDI system in our laboratory. Quantization noise was then added to the model to determine a theoretical SNR as a function of bit-depth. Experimental results were obtained to model and experimentally measure the system SNR, dynamic range, and sensitivity using a high bit-depth acquisition system, for which quantization noise was minimal and could be ignored. Using these results as a baseline, the experimental data were reprocessed at various bit-depths by condensing the number of quantization levels in software and then evaluating the resulting SNR, dynamic range, and sensitivity. Because the other noise terms are analog in origin, changes in these parameters were predominantly attributed to quantization noise and the effects of reduced bit-depth acquisition. The analog noise terms were then added to a theoretical model for quantization noise to determine a theoretical SNR as a function of bit-depth. We then confirmed broad agreement between the theoretical predictions and empirical measures of image quality as a function of bit-depth.

For this analysis, we characterized the system performance using the measured SNR from a calibrated reflector in the sample arm. The SNR was measured as the ratio between the peak

NIH-PA Author Manuscript

NIH-PA Author Manuscript

NIH-PA Author Manuscript

of the signal point spread function to the average noise floor [1,20,21]. The average noise floor was calculated in a region where there was no signal component. Averaging flattened the noise floor by ~0.4 dB. Alternate definitions of the SNR use the mean plus the standard deviation of the noise floor [15,22]. When the system noise is primarily set by the reference arm and not signal arm dependent, the SNR is proportional to the signal arm power. Thus, as long as this condition was preserved, the highest observed SNR served as a lower bound on the system's dynamic range. The system sensitivity was calculated from the measured SNR and the known reflectivity of the sample.

3. Noise analysis

3.1 OFDI noise

Several groups have analyzed the noise in OFDI and have shown the sensitivity advantage of Fourier domain techniques over time-domain OCT [1,2,10,11]. The noise analysis and experimental method used in this paper follows the treatment found in Chen et. al [19], that describes the effect of spectrally balanced detection for OCT data acquisition. The detected current signal in OFDI is given by

$$I=I_{\mathrm{ref}}+I_{\mathrm{sam}}+2^{*}\sqrt{I_{\mathrm{ref}}{}^{*}I_{\mathrm{sam}}}\cos(2\mathrm{kz}) \tag{1}$$

Three noise sources dominate in OFDI: thermal/electrical, shot noise, and relative intensity noise (RIN). Each term is often written in units of A^2/Hz and the total noise given as

$$\sigma_n^2=\sigma_{\mathrm{th}}^2+\sigma_{\mathrm{shot}}^2+\sigma_{\mathrm{RIN}}^2+\sigma_{\mathrm{DAQ}}^2 . \tag{2}$$

The thermal/electrical noise comes from the detector and, in general, is not signal dependent. Shot noise arises from the statistical nature of photons and is given by

$$\sigma_{\mathrm{shot}}^2=2e\left(\frac{\eta e}{h\nu}\right)(P_{\mathrm{ref}}+P_{\mathrm{sam}}) , \tag{3}$$

where e is the electrical charge, η the quantum efficiency of the detector, h Plank's constant, and ν the frequency of the laser light. The RIN noise is due to fluctuations in the laser power:

$$\sigma_{\mathrm{RIN}}^2=\left(\frac{\eta e}{h\nu}\right)^2\tau_{\mathrm{coh}}(P_{\mathrm{ref}}+P_{\mathrm{sam}})^2, \tag{4}$$

where τ_{coh} is the coherence function of the laser. Lasers with narrow instantaneous line widths generally have larger RIN compared with more broadband lasers.

Two additional noise terms are present in OFDI, DAQ noise and quantization noise. DAQ noise is a function of the maximum voltage on the DAQ board but is not dependent on the electrical input signal. Typically, noise figures for DAQ boards are listed as a fraction of the least significant bit (LSB) and result from electronic noise within the DAQ circuitry. As the maximum allowable voltage range (Vmax) of the DAQ increases, the voltage of the LSB increases and the absolute noise value increases proportionally. In most systems, the thermal and DAQ noise terms are much smaller than the other noise terms. With the reference power much higher than the reflected power from the sample arm ($P_{ref} \gg P_{sam}$), the system can approach a shot noise limited sensitivity given by

NIH-PA Author Manuscript

NIH-PA Author Manuscript

NIH-PA Author Manuscript

$$\text{Sensitivity}[\text{dB}] = -10\log\left(\frac{\eta P_{\text{sam}}}{h\nu f_A}\right). \tag{5}$$

3.2 Quantization noise

Quantization noise is induced through distortions caused by the finite bit-depth of the DAQ board. Upon digitization, the analog signal is converted to a digital signal with a finite bit-depth. The number of distinct quantization levels is given by 2^b where b is the number of bits in the DAQ. The spacing of these levels is determined by the full scale voltage range and given by

$$\Delta = \frac{V_{\max}}{2^b}. \tag{6}$$

The process of quantization introduces a detection error that is often modeled as additive noise to the noise terms discussed above [23]. Quantization noise is frequently modeled as white noise with a total noise power given by

$$\sigma_{\text{qn}}^2 = \frac{\Delta^2}{12}. \tag{7}$$

The spectral noise density can be calculated by dividing the total quantization noise power by the detection bandwidth. This model is valid when the quantization noise is uncorrelated with the input sequence and the error probability density function is uniform over the quantization range. In addition, the model of quantization error is suitable for quasi-random input signals which are large relative to the LSB. The model breaks down, however, for small signals when the amplitude of the signal does not cross several quantization levels from sample to sample [23].

4. Experiments

4.1 OFDI System

The OFDI system used in this analysis was used in [8] and described in [1,7]. Briefly, the source consisted of a 40 kHz wavelength swept laser with 143 nm tuning range and an 0.156 nm instantaneous linewidth. Light from the laser was split into a reference and sample arm and recombined and detected using a polarization diverse receiver. An acousto-optic frequency shifter was incorporated into the reference arm to extend the ranging depth [24]. Each channel of the polarization diverse receiver was detected with a dual-balanced detector (ThorLabs PDB110C) and sampled at 85 MS/s with 14-bit resolution (Signatec PDA14) such that there with 2048 samples/A-line. A schematic of the system is shown in Fig. 1. The analysis below follows the noise for only one channel of the polarization diverse detection.

4.2 Noise measurements

The individual noise terms discussed above were measured as follows. First, the DAQ and thermal noise of the detector were measured by blocking both the reference and sample arms. The DAQ noise was measured by terminating the DAQ input at 50-Ohms and digitizing the signal with three values of V_{max} (3V, 1.6V, 1V). The thermal noise was then determined by digitizing the signal from the detector (Thorlabs PDB110C) while the optical signals were blocked, and subtracting the DAQ noise component. The results are shown in Fig. 2. All noise

NIH-PA Author Manuscript

NIH-PA Author Manuscript

NIH-PA Author Manuscript

values were converted to $10*log_{10}(pA^2/Hz)$ so that they could be compared with the optical shot and RIN noise terms. It can be seen that the thermal noise of the detector was roughly 10–20 dB greater than the DAQ noise for all values of Vmax. The average thermal noise between 15 and 25 MHz was 3.6 pA/√Hz which compares very well with the manufacturer's detector specification of 3.8 pA/√Hz. The theoretical quantization noise at 3V V_{max} was −8.5 pA^2/Hz which was nearly 10 dB lower than the measured DAQ noise. This trend held true for all values of V_{max}. Hence, the quantization noise was ignored. The spikes in the DAQ noise measurements were fixed pattern noise of unknown origin. We suspect they are the result of aliased harmonics of the sampling frequency as no signal was input on the DAQ during these measurements.

Next the shot and RIN noise terms were measured by keeping the sample arm blocked and varying the reference arm power with a series of ND filters. After digitization, the DAQ and thermal noise terms were subtracted and the remaining noise was fit to the following equation

$$\sigma_n^2=\gamma 2e(\frac{\eta e}{h\nu})P_{\text{ref}}+P_{\text{RIN}}(\frac{\eta e}{h\nu})^2(P_{\text{ref}})^2 \quad (8)$$

Here P_{RIN} is a fit factor that represents both the coherence function of the laser and the dual-balanced RIN noise reduction and γ is a correction factor that accounts for differences in the detector quantum efficiency used in the fit and aliasing effects. The result of the fit is shown in Fig. 3 with γ equal to 0.83 and P_{RIN} equal to 2.48E-15. The fit and the experimental result match very well for reference powers ranging from 20 to 180 μW. Quantization noise was not included in this fit because the data was digitized at 14 bits and the quantization noise was small relative to the shot and RIN noise terms.

4.3 Bit-depth reduction

With the optical and electrical noise terms well characterized, we proceeded to analyze the effect of quantization noise as a function of bit-depth. The sample arm light was directed to a fixed mirror near the zero delay point. The reference arm power was set at 17.5 μW per channel on the dual balanced receiver, which maximized the sensitivity [1]. The sample arm power was controlled using a series of neutral density (ND) filters. For each measurement, a background signal was collected by blocking the sample arm. After digitization, the background signal was subtracted, the signal was frequency shifted, interpolated, and Fourier transformed to assess the SNR [24].

SNR was evaluated at bit-depths ranging from the original 14 bit acquisition down to 6 bits in 1 bit increments as follows. The original data from the DAQ board was read out as an index value ranging from 1 to 2^{14}. The index value was converted to a voltage using the known Vmax and Δ quantization spacing for 14 bits. For each bit level, a new Δ was calculated and a resampled voltage was generated using

$$V' = \lfloor V/\Delta_b \rfloor * \Delta_b \quad (9)$$

where ⌊ ⌋ represents the floor function and Δ_b the Δ at each bit depth. This transformation was performed on both the background and signal measurements prior to analysis. Alternatively, this process can be thought of as condensing the 2^{14} quantization levels into 2^b levels using

$$\text{Index}' = \text{Index} - \text{rem}(\text{Index}/\text{bitRatio}) \quad (10)$$

where the $bitRatio = 2^{14}/2^b$.

NIH-PA Author Manuscript

NIH-PA Author Manuscript

NIH-PA Author Manuscript

Four data sets at different sample arm attenuations were collected and the Vmax was set at 1V for all the data shown in Fig. 4. A series of 512 A-lines were collected for each sample arm attenuation and the SNR was measured at varying bit-depths. The numbers above each data set give the total attenuation in dB (44.3 dB corresponded to a sample arm power of 0.28 μW at the receiver). The maximum measured sensitivity was 106.9, 107.0, 107.2 and 105.3 dB for the four data sets respectively. Over the entire range of sample arm attenuation values, the noise was dominated by the reference arm power and the SNR was proportional to the sample arm power. Therefore, a lower bound on the system dynamic range was 63.6 dB at 14 bits and 63.0 dB at 8 bits. At higher values of Vmax the quantization noise increased and the SNR attenuation with bit depth was more pronounced. For instance, the SNR was 63.3 dB at 14 bits and 59.9 dB at 8 bits for a Vmax of 3V. However, assuming no other noise sources changed, adjusting the gain on the detector by a factor of 3 would make the quantization noise equal for 3V and 1V Vmax cases such that the SNR rolloff would be identical to that shown in Fig. 4.

Overall, there was a high degree of correlation between the model and experimental measurements ($r = 0.9986$). However, we observed discrepancies between the model and measurement at high bit-depths and at low bit-depths. The discrepancy at high bit depths was most pronounced for high values of attenuation. This effect may be due to the decreased accuracy of k-space interpolation at the lower SNR values. We attribute the discrepancy at low bit depths to a breakdown in the validity of the quantization noise model when the signal no longer crosses multiple quantization levels from sample to sample. This would lead to an overestimate of the quantization noise and an underestimate of the SNR. This effect is more pronounced at higher values of Vmax where the quantization levels are farther apart. Figure 5 shows the SNR loss as a function of bit-depth for each data set. At 8 bits, the loss was ~0.6 dB. The maximum observed loss was 5.5 dB at 6 bits at a sample arm attenuation of 43.3 dB.

5. *In vivo* imaging

In order to test whether a reduced bit-depth acquisition would be sufficient for high quality OFDI images, we reprocessed a data set from a prior human coronary artery imaging study conducted by our laboratory [9]. In this study, the OFDI data was digitized natively at 14 bits. Each A-line was bit-depth reduced in the manner described above. Figure 6 shows a sample frame. The images are displayed in 8-bit grayscale, but all the numerical analysis is done on the full 14 or 8-bit data. A calcific nodule (arrow) can be seen in the lower right hand corner of the image. Even though the image dynamic range was high, there was little, if any, observable qualitative difference between the two images. Following image normalization, the root mean squared error (RMSE) difference between the two images was 2.4 dB and the mean absolute error was 1.7 dB which is in good agreement with the noise model and the experimental results from a single reflector. This error is likely to be negligible for both qualitative assessment and quantitative analysis.

A second reprocessed frame is shown in Fig. 7. This frame was chosen because it contained stent struts, which are metal and have a very high reflectivity. The reflectivity from the struts should provide an upper bound on the dynamic range that an OFDI system will encounter. Following image normalization, the RMSE difference between the two images was 2.3 dB and the mean absolute error was 1.5 dB indicating that reduced bit-depth images can still achieve high dynamic range.

6. Discussion

At increasingly higher OFDI imaging speeds, data transfer and data management demands become a limiting factor when building clinical imaging systems with the highest frame rates. In this paper, we analyzed the system SNR, sensitivity, and dynamic range as a function of

NIH-PA Author Manuscript

NIH-PA Author Manuscript

NIH-PA Author Manuscript

acquisition bit-depth. We compared experimental results of the SNR from a fixed reflector to an OFDI noise model that included optical, electrical, and quantization noise terms. We showed that at 8 bits the experimental loss is approximately 0.6 dB which is in good agreement with the theory. Based on our experience, if the system's sensitivity exceeds 105 dB, then this loss may be considered to be minimal. We also reprocessed OFDI frames from a human coronary artery imaging study and showed that the qualitative assessment and quantitative analysis of image quality at 8-bit was high.

Achieving good image quality at 8-bits has important implications for higher speed OFDI systems, as there are 8-bit DAQ boards capable of sampling at rates of 2 GHz (GageApplied Cobra) that are commercially available. Increased sampling rates allow for increased A-line rates in OFDI imaging. Another possible use of increased sampling speed is to eliminate the need for interpolation into k-space prior to Fourier transform in the image analysis. If the sampling rate was fast enough, even sampling in k-space could be accomplished by picking out a predetermined set of data points without the need for interpolation. It is our experience that these interpolation steps take roughly half to three-quarters of the processing time and increased sampling rates could thereby speed processing rates. More analysis is needed to determine the sampling rates necessary to achieve evenly spaced k-space values for a given laser configuration and is beyond the scope of this paper. This can also be accomplished by using a swept laser that is linear in k-space [25]. In addition, reducing the acquisition bit-depth can lower the data transfer demands for an equivalent speed OFDI at higher bit-depth.

A reduction in acquisition bit-depth can be accomplished in various ways with different tradeoffs. In this paper we performed bit-depth reduction in software. Some commercially available DAQ cards such as the Signatec board used in this study allow for data to be digitized at high bit depth, followed by removal of the low order bits in firmware prior to transfer across the peripheral component interconnect (PCI) bus. Therefore these boards can generate true 8-bit data which could allow for a doubling of the A-line rate or a reduction by half of the data management demand at the same A-line rate. These boards have sampling rates in the 100–200 MS/s range.

In order to achieve an order of magnitude increase in the sampling rate to the GHz range, most commercially available DAQ boards have 8-bit maximum bit-depths. However, with all DAQ boards, the more important number is the effective number of bits (ENOB). The ENOB indicates that the DAQ is equivalent to an ideal DAQ with the corresponding ENOB. The ENOB is calculated by measuring the signal to noise and distortion ratio (SINAD) which is the ratio of the signal amplitude to the sum of all other spectral components including harmonics. The ENOB is then calculated as ENOB = (SINAD – 1.76)/6.02 [26]. For an 8-bit board, the ENOB can be as high as 7.4 bits at sampling rates of 1 or 2 GHz (GageApplied Cobra). This will increase the SNR loss by between 0 and 1 dB. In addition, the shot noise limited sensitivity is reduced at higher A-line rates as seen in Eq. (5). This drop in sensitivity can be overcome by increasing the sample arm power. Other high-speed DAQ boards in the GHz range can digitize at 10-bits with an ENOB as high as 7.8 at 1.7 Gs/s (Pentek 6826002P). In order to overcome the word length constraint of most computers, these boards would need to either drop the low order bits in firmware or be used with custom field-programmable gate array processers with variable word lengths. There may be other factors that affect a hardware based reduction in bit-depth such as offset, non-linearity, and gain error. We don't anticipate this to be a major issue because these errors are often less than one LSB.

We have shown that intensity based OFDI images do not suffer from reduced image quality at 8-bits compared with 14-bit acquisition. One limitation of this technique is that phase based measurements such as polarization or Doppler techniques may suffer from additional loss.

NIH-PA Author Manuscript

NIH-PA Author Manuscript

NIH-PA Author Manuscript

However, the sensitivity of Doppler measurements are related to √SNR such that the loss could be minimized [27].

In addition, Vmax was selected to match the maximum expected voltage range of the OFDI signal. This reduces the quantization noise to its lowest level while still maintaining high dynamic range. In tissue imaging, the maximum signal is not known *a priori* and a highly backscattering signal could in principle exceed Vmax. As discussed above, increasing Vmax will increase the quantization noise and introduce higher SNR loss at decreased bit-depth. We do not believe this to be a major limitation because high quality OFDI images rarely exceed 50 dB of dynamic range and we have demonstrated that at least 63.0 dB of dynamic range at 8-bits is achievable.

7. Conclusion

The advancement of high-speed OFDI presents challenges with data transfer rates and data storage which can limit the practical imaging speed of such systems. We have shown that reduced bit-depth acquisition for OFDI can achieve high system sensitivity with only a minimal drop in the signal-to-noise ratio of ~0.6 dB. The use of reduced bit-depth acquisition can be used to increase the system A-line rate with the same data transfer demands, or to reduce the data management requirement for a given system. This may allow clinical OFDI system to increase their imaging speed without being limited by data transfer rates across the PCI bus.

Acknowledgments

Funding for this work was provided in part by the NIH (1 F31 EB005141–01), Terumo Medical Corporation, NIH R01HL076398, and DOD, the AFOSR MFEL Program (FA9550-04-1-0079).

References and links

1. Yun SH, Tearney GJ, de Boer JF, Iftimia N, Bouma BE. High-speed optical frequency-domain imaging. Opt. Express 2003;11(22):2953–2963. [PubMed: 19471415]
2. Choma M, Sarunic M, Yang C, Izatt J. Sensitivity advantage of swept source and Fourier domain optical coherence tomography. Opt. Express 2003;11(18):2183–2189. [PubMed: 19466106]
3. de Boer JF, Srinivas SM, Park BH, Pham TH, Chen ZP, Milner TE, Nelson JS. Polarization effects in optical coherence tomography of various biological tissues. IEEE J. Sel. Top. Quantum Electron 1999;5(4):1200–1204.
4. Oh WY, Yun SH, Vakoc BJ, Shishkov M, Desjardins AE, Park BH, de Boer JF, Tearney GJ, Bouma BE. High-speed polarization sensitive optical frequency domain imaging with frequency multiplexing. Opt. Express 2008;16(2):1096–1103. [PubMed: 18542183]
5. Zhao Y, Chen Z, Saxer C, Xiang S, de Boer JF, Nelson JS. Phase-resolved optical coherence tomography and optical Doppler tomography for imaging blood flow in human skin with fast scanning speed and high velocity sensitivity. Opt. Lett 2000;25(2):114–116. [PubMed: 18059800]
6. Vakoc B, Yun S, de Boer J, Tearney G, Bouma B. Phase-resolved optical frequency domain imaging. Opt. Express 2005;13(14):5483–5493. [PubMed: 19498543]
7. Yun SH, Tearney GJ, Vakoc BJ, Shishkov M, Oh WY, Desjardins AE, Suter MJ, Chan RC, Evans JA, Jang I-K, Nishioka NS, de Boer JF, Bouma BE. Comprehensive volumetric optical microscopy in vivo. Nat. Med 2006;12(12):1429–1433. [PubMed: 17115049]
8. Suter MJ, Vakoc BJ, Yachimski PS, Shishkov M, Lauwers GY, Mino-Kenudson M, Bouma BE, Nishioka NS, Tearney GJ. Comprehensive microscopy of the esophagus in human patients with optical frequency domain imaging. Gastrointest. Endosc 2008;68(4):745–753. [PubMed: 18926183]
9. Tearney GJ, Waxman S, Shishkov M, Vakoc BJ, Suter MJ, Freilich MI, Desjardins AE, Oh W-Y, Bartlett LA, Rosenberg M, Bouma BE. Three-Dimensional Coronary Artery Microscopy by Intracoronary Optical Frequency Domain Imaging. J Am Coll Cardiol Img 2008;1:752–761.

NIH-PA Author Manuscript

NIH-PA Author Manuscript

NIH-PA Author Manuscript

10. de Boer JF, Cense B, Park BH, Pierce MC, Tearney GJ, Bouma BE. Improved signal-to-noise ratio in spectral-domain compared with time-domain optical coherence tomography. Opt. Lett 2003;28 (21):2067–2069. [PubMed: 14587817]
11. Leitgeb R, Hitzenberger C, Fercher A. Performance of fourier domain vs. time domain optical coherence tomography. Opt. Express 2003;11(8):889–894. [PubMed: 19461802]
12. Yun SH, Boudoux C, Tearney GJ, Bouma BE. High-speed wavelength-swept semiconductor laser with a polygon-scanner-based wavelength filter. Opt. Lett 2003;28(20):1981–1983. [PubMed: 14587796]
13. Oh WY, Yun SH, Tearney GJ, Bouma BE. 115 kHz tuning repetition rate ultrahigh-speed wavelength-swept semiconductor laser. Opt. Lett 2005;30(23):3159–3161. [PubMed: 16350273]
14. Oh WY, Yun SH, Vakoc BJ, Tearney GJ, Bouma BE. Ultrahigh-speed optical frequency domain imaging and application to laser ablation monitoring. Appl. Phys. Lett 2006;88(10):103902–103903.
15. Huber R, Wojtkowski M, Fujimoto JG. Fourier Domain Mode Locking (FDML): A new laser operating regime and applications for optical coherence tomography. Opt. Express 2006;14(8):3225–3237. [PubMed: 19516464]
16. Tomlins P, Wang R. Theory, developments and applications of optical coherence tomography. J. Phys. D 2005;38(15):2519–2535.
17. Yasuno Y, Makita S, Endo T, Aoki G, Sumimura H, Itoh M, Yatagai T. One-shot-phase-shifting Fourier domain optical coherence tomography by reference wavefront tilting. Opt. Express 2004;12 (25):6184–6191. [PubMed: 19488262]
18. Huber R, Adler DC, Fujimoto JG. Buffered Fourier domain mode locking: Unidirectional swept laser sources for optical coherence tomography imaging at 370,000 lines/s. Opt. Lett 2006;31(20):2975–2977. [PubMed: 17001371]
19. Chen Y, de Bruin DM, Kerbage C, de Boer JF. Spectrally balanced detection for optical frequency domain imaging. Opt. Express 2007;15(25):16390–16399. [PubMed: 19550929]
20. Yun SH, Tearney GJ, Bouma BE, Park BH, de Boer JF. High-speed spectral-domain optical coherence tomography at 1.3 mum wavelength. Opt. Express 2003;11(26):3598–3604. [PubMed: 19471496]
21. Lim H, de Boer JF, Park BH, Lee EC, Yelin R, Yun SH. Optical frequency domain imaging with a rapidly swept laser in the 815–870 nm range. Opt. Express 2006;14(13):5937–5944. [PubMed: 19516763]
22. Choma M, Hsu K, Izatt J. Swept source optical coherence tomography using an all-fiber 1300-nm ring laser source. J. Biomed. Opt 2005;10(4):044009.
23. Oppenheim, AV.; Shafer, RW. Discrete-Time Signal Processing. Vol. 2nd ed. Upper Saddle River, NJ: Prentice-Hall, Inc; 1999.
24. Yun S, Tearney G, de Boer J, Bouma B. Removing the depth-degeneracy in optical frequency domain imaging with frequency shifting. Opt. Express 2004;12(20):4822–4828. [PubMed: 19484034]
25. Eigenwillig CM, Biedermann BR, Palte G, Huber R. K-space linear Fourier domain mode locked laser and applications for optical coherence tomography. Opt. Express 2008;16(12):8916–8937. [PubMed: 18545605]
26. Analog Devices, I. Data Conversion Handbook. Newnes: 2004.
27. Park B, Pierce MC, Cense B, Yun S-H, Mujat M, Tearney G, Bouma B, de Boer J. Real-time fiber-based multi-functional spectral-domain optical coherence tomography at 1.3 microm. Opt. Express 2005;13(11):3931–3944. [PubMed: 19495302]

NIH-PA Author Manuscript
NIH-PA Author Manuscript
NIH-PA Author Manuscript

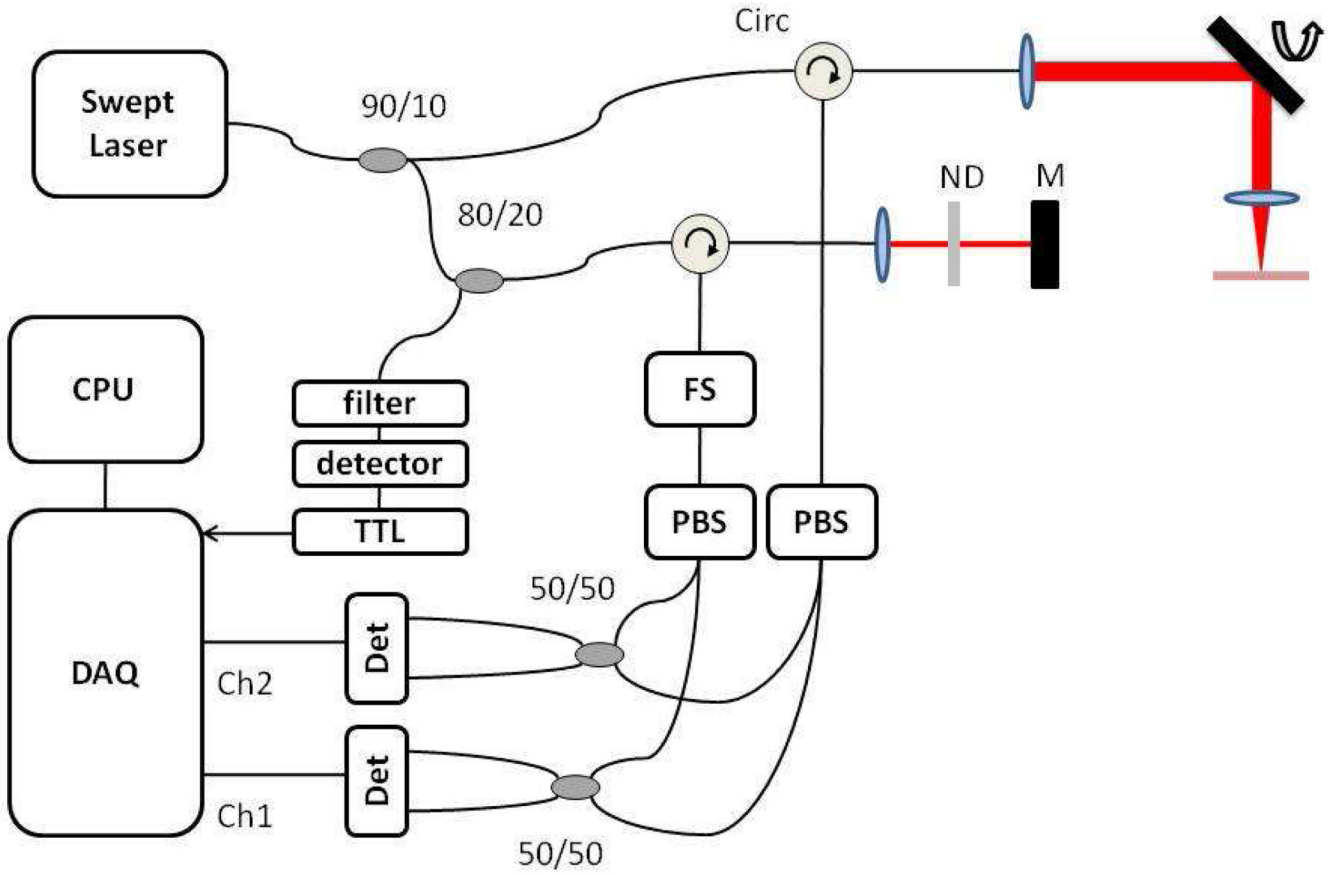

Fig. 1.

OFDI system schematic. The output of a wavelength swept laser was directed to sample and reference arms via a 90/10 coupler. The sample arm consisted of a benchtop galvo scanner for fixed sample imaging. The reference consisted of an ND filter and a fixed mirror as well as an 80/20 coupler to generate a TTL pulse for DAQ board triggering. The reference arm contained a frequency shifter (FS). Both reference and sample arms contained free space polarization beam splitters (PBS). The arms were recombined with 50/50 couplers and sent to two dual balanced receivers.

NIH-PA Author Manuscript
NIH-PA Author Manuscript
NIH-PA Author Manuscript

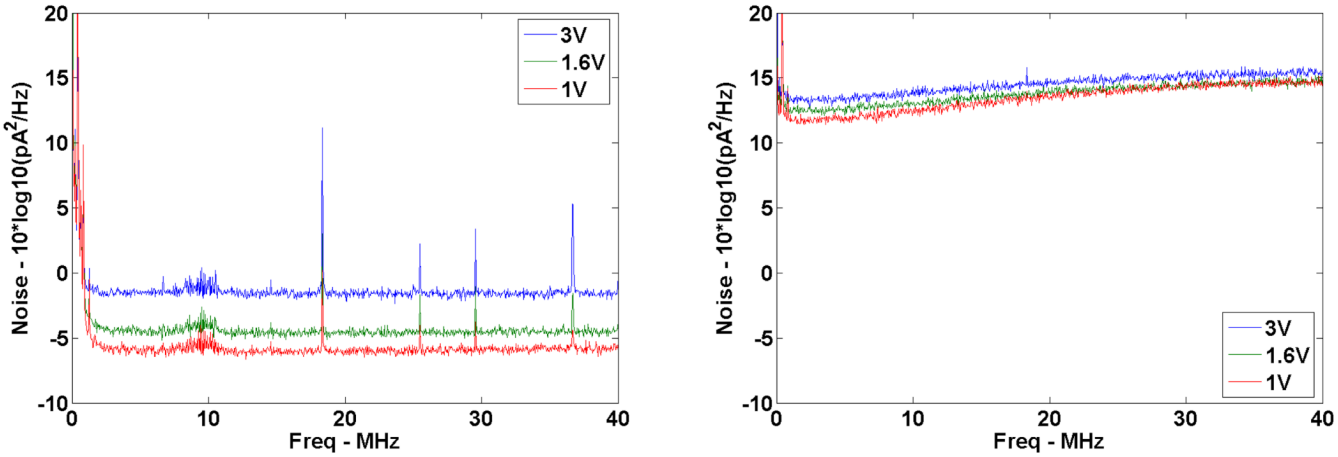

Fig. 2.
DAQ noise (left) and DAQ plus thermal noise (right) measurements at 3,1.6, and 1V Vmax. Noise values are shown in units of $10*log_{10}(pA^2/Hz)$.

NIH-PA Author Manuscript
NIH-PA Author Manuscript
NIH-PA Author Manuscript

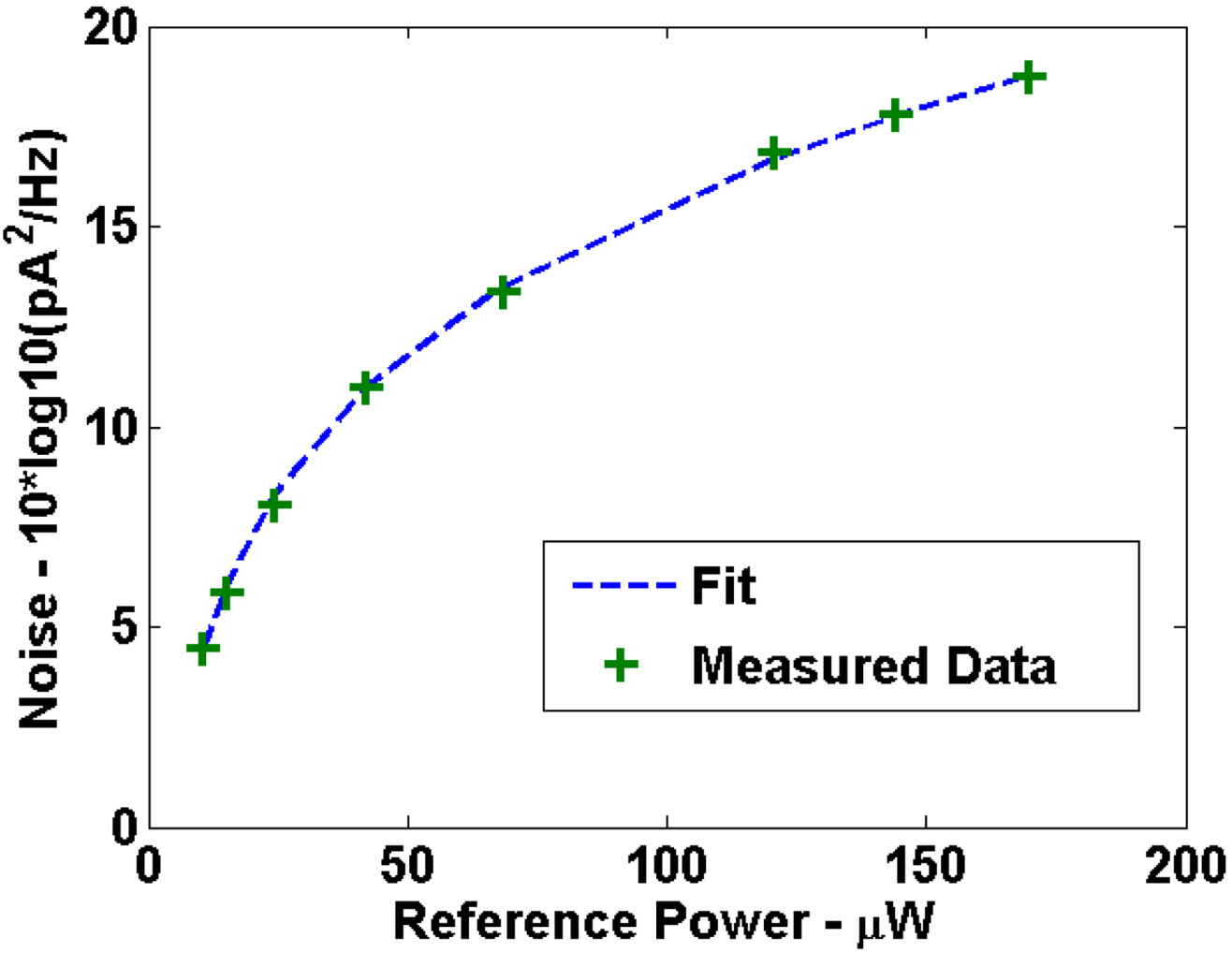

Fig. 3.

Shot plus RIN noise as a function of reference arm power. The dashed line is the fit to Eq. (8) with γ equal to 0.83 and P_{RIN} equal to 2.48E-15. Measured data points are shown as green crosses. Noise is displayed in units of $10*log_{10}(pA^2/Hz)$.

NIH-PA Author Manuscript
NIH-PA Author Manuscript
NIH-PA Author Manuscript

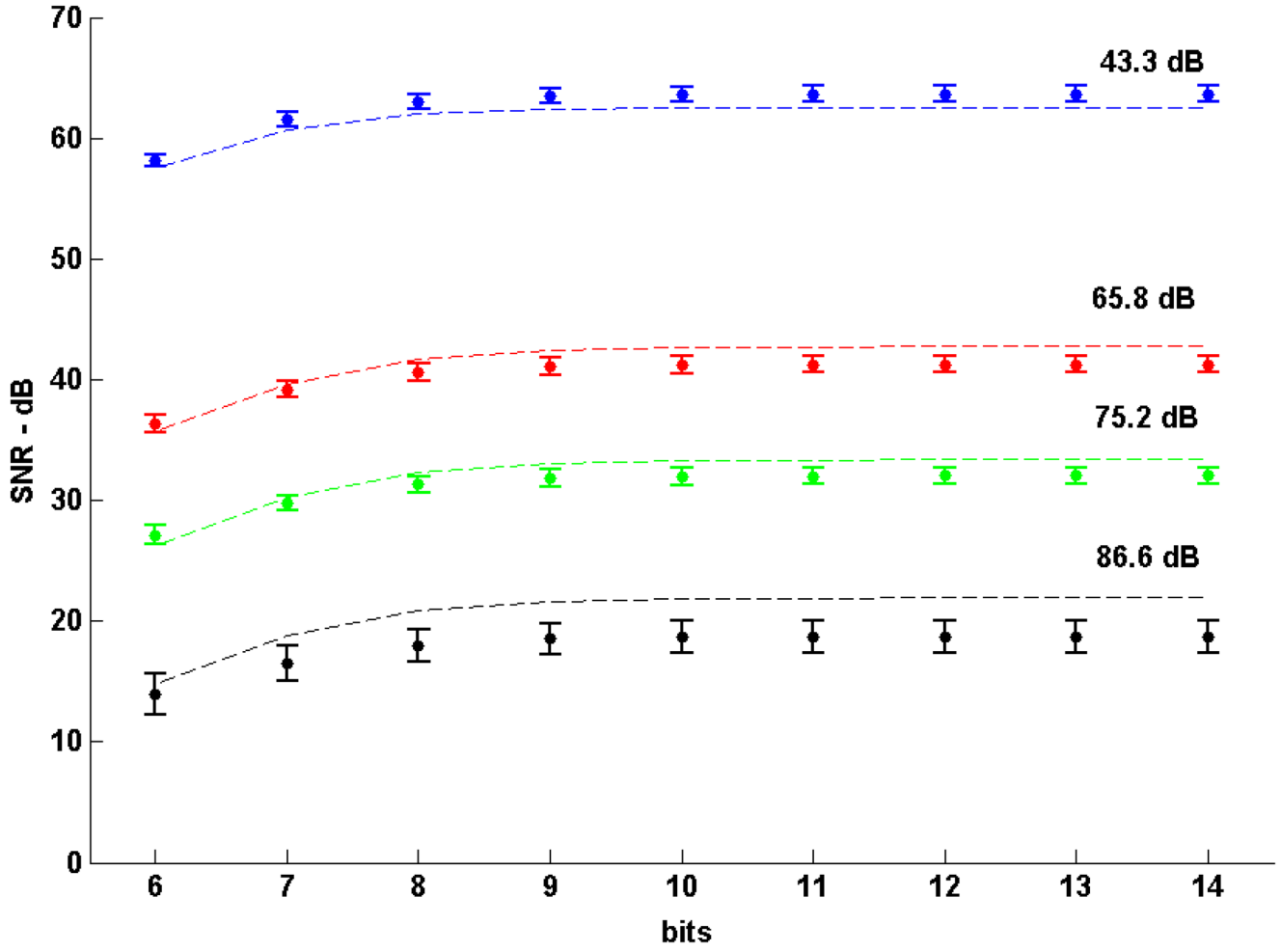

Fig. 4.

SNR as a function of bit-depth from 6 to 14 bits at four sample arm attenuation levels (44.3,65.8,75.2,86.6 dB) and a 1V Vmax. Dashed lines are theoretical SNR values using the measured shot, RIN, thermal, and DAQ noises along with the quantization noise model. Measured values are shown as closed circles with error bars representing the standard deviation.

NIH-PA Author Manuscript
NIH-PA Author Manuscript
NIH-PA Author Manuscript

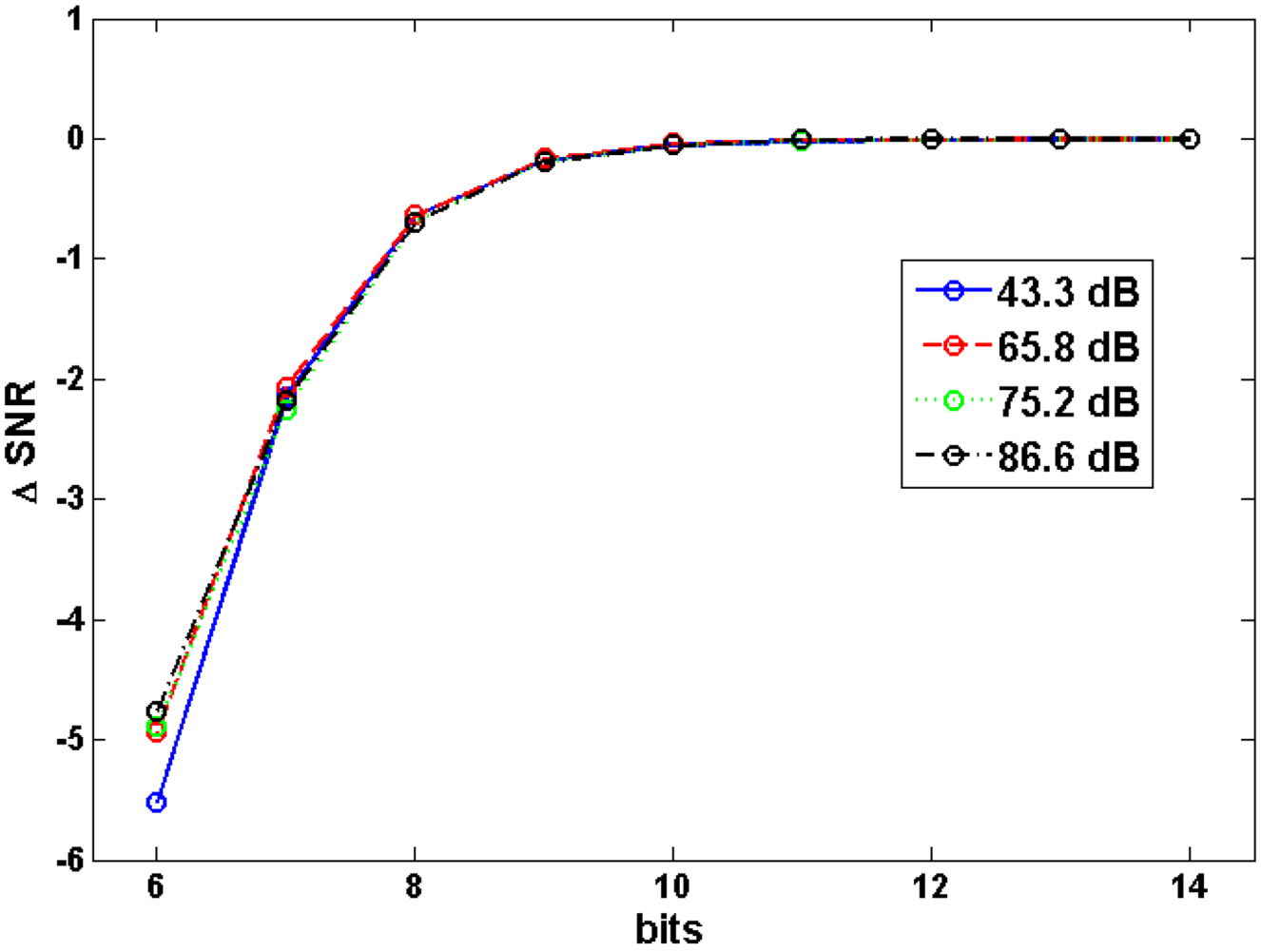

Fig. 5.

Change in SNR as a function of bit-depth. The same sample arm attenuation values are used as in Fig. 4. The curves overlap up to 8 bits and cannot be distinguished. The SNR loss at 8 bits for all curves is ~0.6 dB.

NIH-PA Author Manuscript
NIH-PA Author Manuscript
NIH-PA Author Manuscript

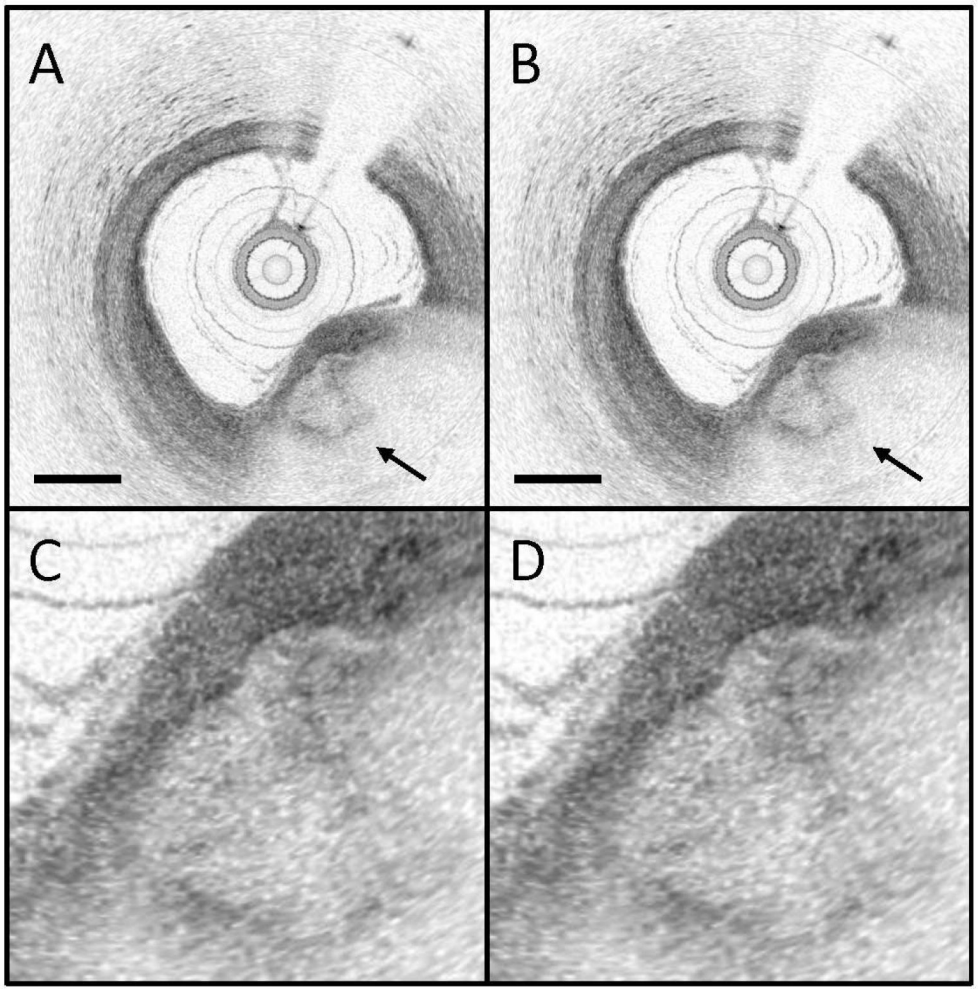

Fig. 6.
Images from a human coronary acquired *in vivo* showing a calcific nodule (arrow). (A) Original (14 bit) data. (B) Reprocessed (8 bit) data. Scale bar, 500 μm. (C) and (D) Zoomed in portion of the calcific nodule.

NIH-PA Author Manuscript
NIH-PA Author Manuscript
NIH-PA Author Manuscript

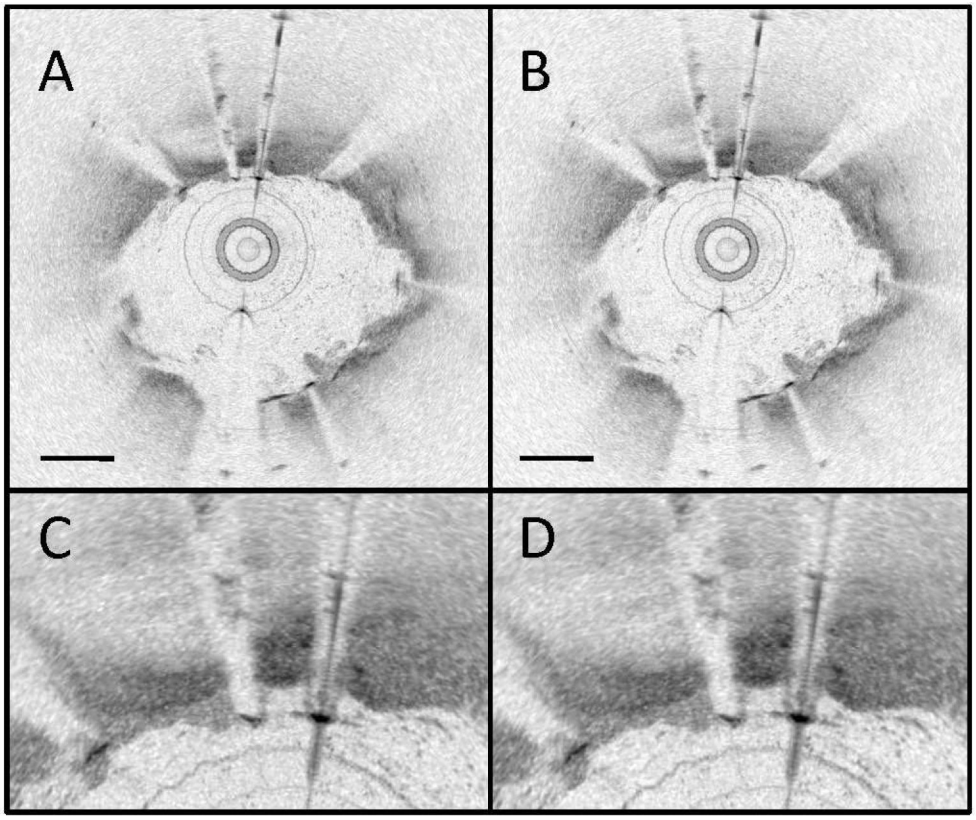

Fig. 7.

Images from a human coronary acquired *in vivo* showing a highly reflective metal stent (A) Original (14 bit) data. (B) Reprocessed (8 bit) data. Scale bar, 500 μm. (C) and (D) Zoomed in section highlighting the high reflection metal stent.